

Conditional Score Guidance for Text-Driven Image-to-Image Translation

Hyunsoo Lee^{*1} Minsoo Kang^{*1} Bohyung Han^{1,2}

¹ECE & ²IPAI, Seoul National University
 {philip21, kminsoo, bhhan}@snu.ac.kr

Abstract

We present a novel algorithm for text-driven image-to-image translation based on a pretrained text-to-image diffusion model. Our method aims to generate a target image by selectively editing the regions of interest in a source image, defined by a modifying text, while preserving the remaining parts. In contrast to existing techniques that solely rely on a target prompt, we introduce a new score function, which considers both a source prompt and a source image, tailored to address specific translation tasks. To this end, we derive the conditional score function in a principled manner, decomposing it into a standard score and a guiding term for target image generation. For the gradient computation, we adopt a Gaussian distribution of the posterior distribution, estimating its mean and variance without requiring additional training. In addition, to enhance the conditional score guidance, we incorporate a simple yet effective mixup method. This method combines two cross-attention maps derived from the source and target latents, promoting the generation of the target image by a desirable fusion of the original parts in the source image and the edited regions aligned with the target prompt. Through comprehensive experiments, we demonstrate that our approach achieves outstanding image-to-image translation performance on various tasks.

1 Introduction

Diffusion models [1–4] have recently shown remarkable performance in various tasks such as unconditional generation of text [5, 6] or image [7, 8] and conditional generation of images [9–11], 3D scenes [12, 13], motion [14, 15], videos [16, 17], or audio [18, 19] given texts and/or images. Thanks to the existence of large-scale labeled examples of text-image pairs [20–24], text-to-image diffusion models [25–29] have achieved outstanding performance. Despite the success of the text-to-image generation models, it is not straightforward to extend the models to text-driven image-to-image translation tasks due to the limited controllability on generated images. For example, in case of the “cat-to-dog” task, the text-to-image diffusion model often fails to focus on the area of cats in a source image for updates and simply generates a totally different dog image.

To sidestep such a critical issue, existing image-to-image translation methods [30–33, 11, 34, 35] based on diffusion models aim to update the semantic contents in a source image specified by a given condition while preserving the region irrelevant to the condition for target image generation. Specifically, [31, 34] fine-tunes the pretrained text-to-image diffusion model so that the distance between the background features in the source and target images is reduced while making the translated image get close to the target domain. On the other hand, [30, 32, 33, 11, 35] revise the

^{*}Equal contribution

generative processes based on diffusion models for the text-to-image generative modeling without extra training.

The main idea of this work is to estimate a score function conditioned on both source image and text in addition to the standard condition with the target text. The new score function is composed of two terms; (a) the standard score function conditioned only on the target prompt and (b) the guiding score function, *i.e.*, the posterior of the source latent given the target latent and the target prompt with respect to the target latent. Note that the posterior is modeled by a Gaussian distribution whose mean and precision matrix are estimated without an additional training process. Also, we employ an effective mixup strategy in cross-attention layers of the text-to-image diffusion model to facilitate image-to-image translation. The main contributions of our paper are summarized below:

- We derive a conditional score and the score can be combined with existing text-to-image diffusion model to guide controllable image generation for image-to-image translation tasks.
- We propose a novel mixup method based on text-to-image diffusion models for image-to-image translation tasks, which combines two outputs of cross-attention layers with inputs as latents of source and target images.
- Experimental results verify that the proposed method achieves outstanding performance on various tasks. To this end, we introduce an intuitive performance evaluation metric, which measures the fidelity of pairwise relations between images before and after translation.

The rest of the paper is organized as follows. Section 2 discusses the related work to text-to-image diffusion models and their application for image-to-image translation tasks. The details of our approach are described in Section 3 and the experimental results are presented in Section 4. Finally, we conclude this paper in Section 5.

2 Related Work

2.1 Text-to-Image Diffusion Models

Diffusion models [1–4] have achieved very promising results on text-to-image generative tasks. For example, Stable Diffusion or Latent Diffusion Models (LDM) [26] employ a two-stage framework [36, 37], where an input image is first projected into a low-dimensional feature using an encoder and a generative model is trained to synthesize the feature while at inference time the image is sampled by generating the representation and then decoding it. In Stable Diffusion, Denoising Diffusion Probabilistic Model (DDPM) [2] is employed for the generative model and a text prompt is represented using a CLIP text encoder [38]. DALL-E 2 [28] consists of two components: a prior model and a decoder. The prior model infers a CLIP image embedding given a text embedding given by a CLIP text encoder while the decoder synthesizes an image conditioned on its CLIP embedding and optionally using textual information. On the other hand, Imagen [25] employs a powerful language encoder [39] trained on text-only corpora for meaningfully represent a text prompt while diffusion models are learned to synthesize an image conditioned on the text embedding.

2.2 Text-Driven Image-to-Image Translation Methods using Diffusion Models

Existing image-to-image translation methods [30–32, 34, 33, 11, 35] aim to preserve the background while editing the object part in the source image. Specifically, Stochastic Differential Editing (SDEdit) [30] draws a latent sample by adding Gaussian noise to a source image as a solution of a stochastic differential equation (SDE) at an intermediate time and then synthesizes an image by solving the reverse time of the SDE from the intermediate time to the initial time. On the other hand, DiffusionCLIP [31] fine-tune a pre-trained text-to-image generative network using the local directional loss [40] using a pre-trained CLIP [38] while the L1 reconstruction loss and optionally the face identity loss [41] only for human face image manipulation tasks are also adopted, where all losses are computed using the source and target images. Blended Diffusion [32] requires a background mask provided by a user so that latents of the source and target images are mixed according to the given mask in order to preserve the background while translating the content region into the target domain. On the other hand, Imagic [34] performs fine-tuning for the text-to-image diffusion model conditioned on the inferred text features based on the source image and then simply generates the

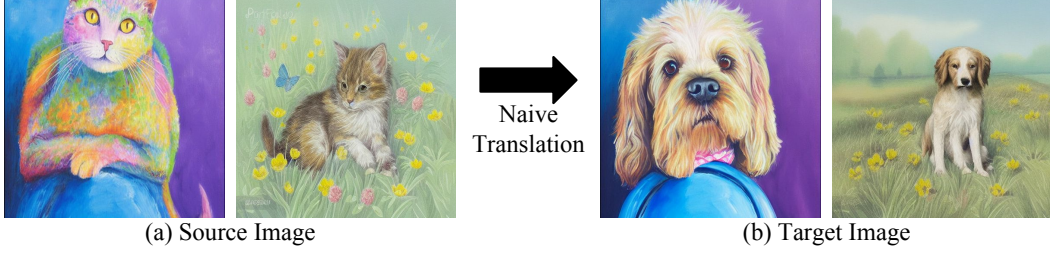


Figure 1: Image translation results of \mathbf{x}^{tgt} using the simple naive generative process in Eq (3).

target image conditioned on the linear combination of the predicted source text feature and its target feature.

3 Framework

This section describes the background for image-to-image translation tasks using diffusion models. Then, we present our derivation of the conditional score function and describe how to apply the conditional score to image-to-image translation tasks. Also, we propose an effective mixup strategy in cross-attention layers to preserve the background while editing the content region. The proposed algorithm is presented in Algorithm 1.

3.1 Preliminary: Image Translation for Diffusion Models

3.1.1 Latent Extraction for Source Images

Diffusion models [1, 2, 4] define a series of latent variables $\mathbf{x}_1, \mathbf{x}_2, \dots, \mathbf{x}_T$ with a predefined number T which share the same dimensionality as the data $\mathbf{x}_0 \in \mathbb{R}^{H \times W \times C}$, where the sampling process of \mathbf{x}_t depends on \mathbf{x}_{t-1} and \mathbf{x}_0 in DDIM [4] while DDPM [2] assumes the data generating process follows a Markov chain. For notational simplicity, we regard the 3D variables as 1-dimensional vectors $\in \mathbb{R}^{HWC}$. For image-to-image translation tasks, existing works [33, 11, 35] often employ a deterministic inference of DDIM instead of a stochastic version of DDPM as follows:

$$\mathbf{x}_{t+1}^{\text{src}} = \sqrt{\alpha_{t+1}} f_{\theta}(\mathbf{x}_t^{\text{src}}, t, \mathbf{y}^{\text{src}}) + \sqrt{1 - \alpha_{t+1}} \epsilon_{\theta}(\mathbf{x}_t^{\text{src}}, t, \mathbf{y}^{\text{src}}), \quad (1)$$

where $\mathbf{x}_t^{\text{src}}$ and $\mathbf{y}_t^{\text{src}}$ are a latent variable of a source image \mathbf{x}^{src} and a textual embedding of a source prompt p^{src} given by pretrained models [39, 38] depending on text-to-image diffusion models [25, 26] while $\alpha_t \in (0, 1]$ is a predefined decreasing sequence. In the above equation, $\epsilon_{\theta}(\cdot, \cdot, \cdot)$ is a noise prediction network based on a U-Net backbone [42] and $f_{\theta}(\cdot, \cdot, \cdot)$ is defined as

$$f_{\theta}(\mathbf{x}_t, t, \mathbf{y}) = \frac{\mathbf{x}_t - \sqrt{1 - \alpha_t} \epsilon_{\theta}(\mathbf{x}_t, t, \mathbf{y})}{\sqrt{\alpha_t}}. \quad (2)$$

The final latent $\mathbf{x}_T^{\text{src}}$ can be recursively sampled using Eq. (1), which is employed for the generation of the target image \mathbf{x}^{tgt} or the reconstruction of the source image \mathbf{x}^{src} .

3.1.2 Naive Generative Process of Target Images

A naive method for image translation tasks using diffusion models simply generates the target image \mathbf{x}^{tgt} given the final latent $\mathbf{x}_T^{\text{tgt}}$, which is equal to $\mathbf{x}_T^{\text{src}}$, using the reverse DDIM process as follows:

$$\mathbf{x}_{t-1}^{\text{tgt}} = \sqrt{\alpha_{t-1}} f_{\theta}(\mathbf{x}_t^{\text{tgt}}, t, \mathbf{y}^{\text{tgt}}) + \sqrt{1 - \alpha_{t-1}} \epsilon_{\theta}(\mathbf{x}_t^{\text{tgt}}, t, \mathbf{y}^{\text{tgt}}). \quad (3)$$

However, as presented in Figure 1, the simple translation algorithm often results in poor generation results in terms of failing to maintain the background region that needs to be fixed in the source image while the structure of the content is also mostly changed. To address this issue, previous approaches employ the information in the reverse process of $\mathbf{x}_t^{\text{src}}$ when synthesizing the target image. Specifically, in order to preserve the part of the region in the source image, Prompt-to-Prompt [33] delivers the cross-attention maps while Plug-and-Play [11] injects the self-attention and intermediate feature

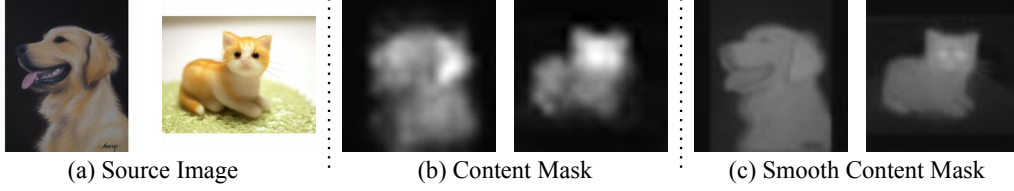


Figure 2: Visualization of the content mask $\mathbf{M}^{\text{src}}[k]$ and its smooth version $\hat{\mathbf{M}}^{\text{src}}$.

maps $\psi_\theta(\mathbf{x}_t^{\text{src}})$ in the noise prediction network during the early steps in the reverse process of $\mathbf{x}_t^{\text{tgt}}$. The attention maps are calculated using a query $\mathbf{Q}_t^{\text{src}}$ and a key $\mathbf{K}_t^{\text{src}}$ as $\text{softmax}\left(\frac{\mathbf{Q}_t^{\text{src}}(\mathbf{K}_t^{\text{src}})^T}{\sqrt{d}}\right)$ during the computation of the reverse process of $\mathbf{x}_t^{\text{src}}$, where d is the last dimension of $\mathbf{Q}_t^{\text{src}}$ and $\mathbf{K}_t^{\text{src}}$. Here, using two linear layers f^{query} and f^{key} , $\mathbf{Q}_t^{\text{src}}$ is computed as $f^{\text{query}}(\psi_\theta(\mathbf{x}_t^{\text{src}}))$ while $\mathbf{K}_t^{\text{src}}$ is determined by $f^{\text{key}}(\psi_\theta(\mathbf{x}_t^{\text{src}}))$ for the self-attention or $f^{\text{key}}(\mathbf{y}^{\text{src}})$ for the cross-attention. For the remaining steps, the reverse DDIM process defined as Eq. (3) is applied to generate the target image without any modification. On the other hand, Pix2Pix-Zero [35] first updates the latent $\mathbf{x}_t^{\text{tgt}}$ by taking a gradient step to reduce the distance between the cross-attention maps given by the reverse process of $\mathbf{x}_t^{\text{src}}$ and $\mathbf{x}_t^{\text{tgt}}$ and then perform the DDIM generation process using the updated latent.

3.2 Cross-Attention Mixup

During the reverse process of $\mathbf{x}_t^{\text{tgt}}$, using the property [33] that the cross-attention plays an important role to control the relation between the spatial layout of the image and each word in the prompt, we aim to estimate a background mask $\mathbf{P}^{\text{src}} \in \mathbb{R}^{H \times W}$ in the range of $[0, 1]$ indicating where to preserve the source image. Specifically, we first compute a cross-attention map \mathbf{M}^{src} that is the average of the cross-attention map $\mathbf{M}_t^{\text{src}} \in \mathbb{R}^{L \times H_1 \times W_1}$ across all timesteps extracted from the noise prediction network whose input is $\mathbf{x}_t^{\text{src}}$. Then, we select the k^{th} spatial map in \mathbf{M}^{src} denoted as $\mathbf{M}^{\text{src}}[k]$, where the k^{th} token in the source prompt contains the information about the semantic region of the source image that needs to be edited. However, the weakness of the direct application about $\mathbf{M}^{\text{src}}[k]$ is that the part of the contents of the interest is much more highlighted than that of the other part. For example, in case of the ‘‘cat-to-dog’’ task, the head region of $\mathbf{M}^{\text{src}}[k]$ related to the word ‘‘cat’’ has large values while the values corresponding to the body parts are relatively low. To address the above issue, we aim to apply a regularization technique to the content mask $\mathbf{M}^{\text{src}}[k]$ for regional smoothness as presented in Figure 2. For the regularization, we exploit the averaged self-attention map $\mathbf{A}^{\text{src}} \in \mathbb{R}^{H \times W \times H \times W}$ extracted from the noise prediction network during the reverse DDIM process. The motivation is that the self-attention map can reflect the structure of the image, where matrices obtained from different regions in the self-attention map are far apart, and vice versa as mentioned in [11]. Moreover, each matrix in the attention map, which corresponds to each pixel, captures the similarity between the corresponding pixel and all other pixels. Using the self-attention map \mathbf{A}^{src} , we compute $\hat{\mathbf{M}}^{\text{src}} \in \mathbb{R}^{H \times W}$ as the smooth version of $\mathbf{M}^{\text{src}}[k]$ as follows:

$$\hat{\mathbf{M}}^{\text{src}}[h, w] = \text{tr}(\mathbf{A}^{\text{src}}[h, w](\mathbf{M}^{\text{src}}[k])^T), \quad (4)$$

where $\text{tr}(\cdot)$ denotes the trace operator while $\mathbf{A}^{\text{src}}[h, w] \in \mathbb{R}^{H \times W}$ and $\hat{\mathbf{M}}^{\text{src}}[h, w] \in \mathbb{R}$ represent the matrix of \mathbf{A}^{src} and the element of $\hat{\mathbf{M}}^{\text{src}}$ located at pixel position (h, w) , respectively. Using the smoothed attention matrix $\hat{\mathbf{M}}^{\text{src}}$, the background mask $\mathbf{P}^{\text{src}} \in \mathbb{R}^{H \times W}$ that needs to be preserved for the image-to-image translation task can be inferred as

$$\mathbf{P}^{\text{src}} = \mathbf{1} - \hat{\mathbf{M}}^{\text{src}}, \quad (5)$$

where $\mathbf{1} \in \mathbb{R}^{H \times W}$ denotes the all-one matrix. Each element of \mathbf{P}^{src} can be interpreted as the probability that the corresponding pixel in the image belongs to the background.

Given the background mask \mathbf{P}^{src} , we propose a new cross-attention guidance method called *cross-attention mixup* as follows:

$$\hat{\mathbf{M}}_t^{\text{tgt}}[\ell] = \mathbf{M}_t^{\text{src}}[\ell] \odot \mathbf{P}^{\text{src}} + \mathbf{M}_t^{\text{tgt}}[\ell] \odot (\mathbf{1} - \mathbf{P}^{\text{src}}), \quad (6)$$

where $\mathbf{M}_t^{\text{tgt}} \in \mathbb{R}^{L \times H_1 \times W_1}$ denotes the cross-attention maps extracted from the noise prediction network using $\mathbf{x}_t^{\text{tgt}}$ as an input. $\mathbf{M}_t^{\text{tgt}}[\ell] \in \mathbb{R}^{H_1 \times W_1}$ and $\mathbf{M}_t^{\text{src}}[\ell] \in \mathbb{R}^{H_1 \times W_1}$ are the spatial maps

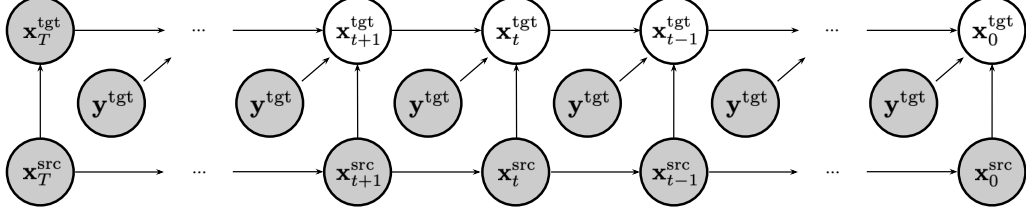


Figure 3: Graphical model of the proposed method about target image generation.

of $\mathbf{M}_t^{\text{tgt}}$ and $\mathbf{M}_t^{\text{src}}$ corresponding to the ℓ^{th} token in the prompts. The motivation of *cross-attention mixup* is to preserve the background while editing only the regions of interest. Specifically, the first term of Eq. (6), $\mathbf{M}_t^{\text{src}}[\ell] \odot \mathbf{P}^{\text{src}}$, represents pixel information to be preserved while the second term, $\mathbf{M}_t^{\text{tgt}}[\ell] \odot (1 - \mathbf{P}^{\text{src}})$, corresponds to a guiding information for the translation into target objects. After performing the mixup in Eq. (6), the noise prediction in the denoising network is given by $\hat{\mathbf{M}}_t^{\text{tgt}}$ instead of $\mathbf{M}_t^{\text{tgt}}$ at every timestep t .

3.3 Conditional Score Estimation

For the conditional reverse process of image-to-image translation, we compute the conditional score $\nabla_{\mathbf{x}_t^{\text{tgt}}} \log p(\mathbf{x}_t^{\text{tgt}} | \mathbf{x}_t^{\text{src}}, \mathbf{y}^{\text{tgt}}, \mathbf{y}^{\text{src}})$, which is given by

$$\begin{aligned} \nabla_{\mathbf{x}_t^{\text{tgt}}} \log p(\mathbf{x}_t^{\text{tgt}} | \mathbf{x}_t^{\text{src}}, \mathbf{y}^{\text{tgt}}, \mathbf{y}^{\text{src}}) &= \nabla_{\mathbf{x}_t^{\text{tgt}}} \log \int p(\mathbf{x}_t^{\text{tgt}}, \mathbf{x}_t^{\text{src}} | \mathbf{x}_t^{\text{src}}, \mathbf{y}^{\text{tgt}}, \mathbf{y}^{\text{src}}) d\mathbf{x}_t^{\text{src}} \\ &= \nabla_{\mathbf{x}_t^{\text{tgt}}} \log \int p(\mathbf{x}_t^{\text{tgt}} | \mathbf{x}_t^{\text{src}}, \mathbf{x}_t^{\text{src}}, \mathbf{y}^{\text{tgt}}, \mathbf{y}^{\text{src}}) \cdot p(\mathbf{x}_t^{\text{src}} | \mathbf{x}_t^{\text{src}}, \mathbf{y}^{\text{tgt}}, \mathbf{y}^{\text{src}}) d\mathbf{x}_t^{\text{src}} \\ &= \nabla_{\mathbf{x}_t^{\text{tgt}}} \log \int p(\mathbf{x}_t^{\text{tgt}} | \mathbf{x}_t^{\text{src}}, \mathbf{y}^{\text{tgt}}) \cdot p(\mathbf{x}_t^{\text{src}} | \mathbf{x}_t^{\text{src}}, \mathbf{y}^{\text{src}}) d\mathbf{x}_t^{\text{src}} \quad (7) \\ &\approx \nabla_{\mathbf{x}_t^{\text{tgt}}} \log p(\mathbf{x}_t^{\text{tgt}} | \hat{\mathbf{x}}_t^{\text{src}}, \mathbf{y}^{\text{tgt}}). \quad (8) \end{aligned}$$

In Eq. (7), $\mathbf{x}_t^{\text{tgt}}$ is independent of \mathbf{y}^{src} and $\mathbf{x}_t^{\text{src}}$ as illustrated in Figure 3 while $\mathbf{x}_t^{\text{src}}$ is irrelevant with respect to \mathbf{y}^{tgt} and $\hat{\mathbf{x}}_t^{\text{src}}$ is a sample drawn from $p(\mathbf{x}_t^{\text{src}} | \mathbf{x}_t^{\text{src}}, \mathbf{y}^{\text{src}})$. We further decompose the right-hand side of Eq. (8) as

$$\nabla_{\mathbf{x}_t^{\text{tgt}}} \log p(\mathbf{x}_t^{\text{tgt}} | \hat{\mathbf{x}}_t^{\text{src}}, \mathbf{y}^{\text{tgt}}) = \nabla_{\mathbf{x}_t^{\text{tgt}}} \log p(\mathbf{x}_t^{\text{tgt}} | \mathbf{y}^{\text{tgt}}) + \nabla_{\mathbf{x}_t^{\text{tgt}}} \log p(\hat{\mathbf{x}}_t^{\text{src}} | \mathbf{x}_t^{\text{tgt}}, \mathbf{y}^{\text{tgt}}), \quad (9)$$

where the first term $\nabla_{\mathbf{x}_t^{\text{tgt}}} \log p(\mathbf{x}_t^{\text{tgt}} | \mathbf{y}^{\text{tgt}})$ is estimated by the noise prediction network as the standard reverse process. Finally, the conditional score we aim to estimate is given by

$$\nabla_{\mathbf{x}_t^{\text{tgt}}} \log p(\mathbf{x}_t^{\text{tgt}} | \mathbf{x}_t^{\text{src}}, \mathbf{y}^{\text{tgt}}, \mathbf{y}^{\text{src}}) \approx \nabla_{\mathbf{x}_t^{\text{tgt}}} \log p(\mathbf{x}_t^{\text{tgt}} | \mathbf{y}^{\text{tgt}}) + \nabla_{\mathbf{x}_t^{\text{tgt}}} \log p(\hat{\mathbf{x}}_t^{\text{src}} | \mathbf{x}_t^{\text{tgt}}, \mathbf{y}^{\text{tgt}}). \quad (10)$$

The remaining issue is how to compute the gradient of the log-posterior $\nabla_{\mathbf{x}_t^{\text{tgt}}} \log p(\hat{\mathbf{x}}_t^{\text{src}} | \mathbf{x}_t^{\text{tgt}}, \mathbf{y}^{\text{tgt}})$, which leads to unique results compared with the simple reverse DDIM method.

3.4 Conditional Score Guidance

We aim to implement the proposed conditional score estimation using the noise prediction network ϵ_θ widely employed in off-the-shelf text-to-image diffusion models [25, 26]. We first derive an equivalent form of the naive reverse DDIM process by plugging Eq. (2) into Eq. (3) as

$$\mathbf{x}_{t-1}^{\text{tgt}} = \frac{\sqrt{\alpha_{t-1}}}{\sqrt{\alpha_t}} \mathbf{x}_t^{\text{tgt}} - \sqrt{1 - \alpha_t} \gamma_t \epsilon_\theta(\mathbf{x}_t^{\text{tgt}}, t, \mathbf{y}^{\text{tgt}}) \approx \frac{\sqrt{\alpha_{t-1}}}{\sqrt{\alpha_t}} \mathbf{x}_t^{\text{tgt}} + (1 - \alpha_t) \gamma_t \nabla_{\mathbf{x}_t^{\text{tgt}}} \log p(\mathbf{x}_t^{\text{tgt}} | \mathbf{y}^{\text{tgt}}), \quad (11)$$

where

$$\nabla_{\mathbf{x}_t^{\text{tgt}}} \log p(\mathbf{x}_t^{\text{tgt}} | \mathbf{y}^{\text{tgt}}) \approx -\frac{1}{\sqrt{1 - \alpha_t}} \epsilon_\theta(\mathbf{x}_t^{\text{tgt}}, t, \mathbf{y}^{\text{tgt}}) \text{ and } \gamma_t = \sqrt{\frac{\alpha_{t-1}}{\alpha_t}} - \sqrt{\frac{1 - \alpha_{t-1}}{1 - \alpha_t}}. \quad (12)$$

Algorithm 1 Conditional Score Guidance with Cross-Attention Mixup

Inputs: A source image \mathbf{x}^{src} , A source prompt embedding \mathbf{y}^{src} , A target prompt embedding \mathbf{y}^{tgt} ,
A weight for the precision matrix λ^{pre}
 $\mathbf{x}_0^{\text{src}} \leftarrow \mathbf{x}^{\text{src}}$
for $t \leftarrow 0, \dots, T-1$ **do**
 Compute $\mathbf{x}_{t+1}^{\text{src}}$ by Eq. (1) while saving $\mathbf{M}_t^{\text{src}}$ and $\mathbf{A}_t^{\text{src}}$
end for
 $\mathbf{x}_T^{\text{tgt}} \leftarrow \mathbf{x}_T^{\text{src}}$
Compute $\bar{\mathbf{M}}^{\text{src}}$ and $\bar{\mathbf{A}}^{\text{src}}$ by averaging $\mathbf{M}_t^{\text{src}}$ and $\mathbf{A}_t^{\text{src}}$ over timesteps
Compute $\bar{\mathbf{M}}^{\text{src}}$ using $\bar{\mathbf{M}}^{\text{src}}$ and $\bar{\mathbf{A}}^{\text{src}}$ by Eq. (4) and $\mathbf{P}^{\text{src}} \leftarrow \mathbf{1} - \bar{\mathbf{M}}^{\text{src}}$ by Eq. (5)
for $t \leftarrow T, \dots, 1$ **do**
 Compute $\hat{\epsilon}_t^{\text{tgt}} \leftarrow \epsilon_\theta(\mathbf{x}_t^{\text{tgt}}, t, \mathbf{y}^{\text{tgt}})$ using cross-attention mixup with $\mathbf{M}_t^{\text{src}}$ and \mathbf{P}^{src} in Eq. (6)
 Compute $\gamma_t \leftarrow \sqrt{\frac{\alpha_{t-1}}{\alpha_t}} - \sqrt{\frac{1-\alpha_{t-1}}{1-\alpha_t}}$ and $\boldsymbol{\Omega}_t$ using Eq. (14) and (15)
 Perform our conditional score guidance using $\hat{\epsilon}_t^{\text{tgt}}$ by Eq. (16):
 $\hat{\mathbf{x}}_t^{\text{src}} \leftarrow \mathbf{x}_t^{\text{src}}$
 $\mathbf{x}_{t-1}^{\text{tgt}} \leftarrow \sqrt{\alpha_{t-1}} \left(\frac{\mathbf{x}_t^{\text{tgt}} - \sqrt{1-\alpha_t} \hat{\epsilon}_t^{\text{tgt}}}{\sqrt{\alpha_t}} \right) + \sqrt{1-\alpha_{t-1}} \hat{\epsilon}_t^{\text{tgt}} - \gamma_t \boldsymbol{\Omega}_t (\mathbf{x}_t^{\text{tgt}} - \hat{\mathbf{x}}_t^{\text{src}})$
end for
 $\mathbf{x}_0^{\text{tgt}} \leftarrow \mathbf{x}_0^{\text{tgt}}$
Output: A target image \mathbf{x}^{tgt}

Note that the score approximation of $\nabla_{\mathbf{x}_t^{\text{tgt}}} \log p(\mathbf{x}_t^{\text{tgt}} | \mathbf{y}^{\text{tgt}})$ is based on the suggestion in [3].

For the computation of $\nabla_{\mathbf{x}_t^{\text{tgt}}} \log p(\hat{\mathbf{x}}_t^{\text{src}} | \mathbf{x}_t^{\text{tgt}}, \mathbf{y}^{\text{tgt}})$, we choose $p(\hat{\mathbf{x}}_t^{\text{src}} | \mathbf{x}_t^{\text{tgt}}, \mathbf{y}^{\text{tgt}}) \sim \mathcal{N}(\mathbf{x}_t^{\text{tgt}}, (1-\alpha_t)\boldsymbol{\Omega}_t^{-1})$ with a diagonal precision matrix $\boldsymbol{\Omega}_t$, which is given by

$$\nabla_{\mathbf{x}_t^{\text{tgt}}} \log p(\hat{\mathbf{x}}_t^{\text{src}} | \mathbf{x}_t^{\text{tgt}}, \mathbf{y}^{\text{tgt}}) = -\frac{\boldsymbol{\Omega}_t(\mathbf{x}_t^{\text{tgt}} - \hat{\mathbf{x}}_t^{\text{src}})}{1 - \alpha_t}, \quad (13)$$

where each diagonal element in $\boldsymbol{\Omega}_t$ has a large precision value if it corresponds to the pixel that should be preserved and consequently has a low variance, and vice versa.

Given the smoothed background mask \mathbf{P}^{src} , we estimate the precision matrix $\boldsymbol{\Omega}_t$ as

$$\boldsymbol{\Omega}_t = \lambda^{\text{pre}} \cdot \mathbf{B}_t \odot \mathbf{P}^{\text{src}}, \quad (14)$$

where \odot denotes the Hadamard product operator while λ^{pre} is a hyperparameter to control the magnitude of each element in $\boldsymbol{\Omega}_t$. In Eq. (14), $\mathbf{B}_t \in \mathbb{R}^{H \times W}$ is a binary matrix dependent on t and \mathbf{P}^{src} , which is defined as

$$\mathbf{B}_t[h, w] = \begin{cases} 0 & \text{if } \mathbf{P}^{\text{src}}[h, w] < 1 - \cos\left(\frac{\pi(T-t)}{T\delta}\right), \\ 1 & \text{otherwise} \end{cases}, \quad (15)$$

where $\mathbf{B}_t[h, w]$ is the entry in the h^{th} row and w^{th} column of \mathbf{B}_t and δ is a hyperparameter that determines the period of the cosine function and set to 1.5. The motivation for introducing \mathbf{B}_t is to ignore the error between the true mean of the posterior $p(\hat{\mathbf{x}}_t^{\text{src}} | \mathbf{x}_t^{\text{tgt}}, \mathbf{y}^{\text{tgt}})$ and its estimate $\mathbf{x}_t^{\text{tgt}}$ since it will increase as t approaches 0 especially for the outside of the background.

The new reverse process guided by the proposed conditional score is formulated by replacing the original score function of the pretrained text-to-image diffusion model, $\nabla_{\mathbf{x}_t^{\text{tgt}}} \log p(\mathbf{x}_t^{\text{tgt}} | \mathbf{y}^{\text{tgt}})$ in Eq. (11), with the one conditioned on a source data, $\nabla_{\mathbf{x}_t^{\text{tgt}}} \log p(\mathbf{x}_t^{\text{tgt}} | \mathbf{x}^{\text{src}}, \mathbf{y}^{\text{tgt}}, \mathbf{y}^{\text{src}})$ in Eq. (10). Then, the following equation is finally derived for our reverse process:

$$\mathbf{x}_{t-1}^{\text{tgt}} = \sqrt{\alpha_{t-1}} f_\theta(\mathbf{x}_t^{\text{tgt}}, t, \mathbf{y}^{\text{tgt}}) + \sqrt{1-\alpha_{t-1}} \epsilon_\theta(\mathbf{x}_t^{\text{tgt}}, t, \mathbf{y}^{\text{tgt}}) - \gamma_t \boldsymbol{\Omega}_t (\mathbf{x}_t^{\text{tgt}} - \hat{\mathbf{x}}_t^{\text{src}}), \quad (16)$$

which has an additional guidance term compared to the original diffusion model shown in Eq. (3).

4 Experiments

This section compares the proposed method, referred to as CSG, with the state-of-the-art methods [33, 35] and the simple reverse DDIM method as mentioned in Section 3.1.2 using the pretrained Stable Diffusion [26]. We also present ablation study results to analyze the proposed components.

Table 1: Quantitative results to compare with text-driven image-to-image translation methods [4, 33, 35] using the pre-trained Stable Diffusion [26] and real images sampled from LAION 5B dataset [20] for various tasks. ‘DDIM’ denotes the simple inference using Eq. (3). Black and red bold-faced numbers represent the best and second-best performance in each row.

Task	DDIM [4]			Prompt-to-Prompt [33]			Pix2Pix-Zero [35]			CSG (Ours)		
	CS (\uparrow)	SD (\downarrow)	RD (\downarrow)	CS (\uparrow)	SD (\downarrow)	RD (\downarrow)	CS (\uparrow)	SD (\downarrow)	RD (\downarrow)	CS (\uparrow)	SD (\downarrow)	RD (\downarrow)
cat \rightarrow dog	0.2921	0.0725	0.4325	0.2907	0.0213	0.0791	0.3015	0.0226	0.1589	0.3014	0.0192	0.0217
dog \rightarrow cat	0.2903	0.0748	0.4608	0.2612	0.0204	0.1947	0.2954	0.0220	0.3229	0.2958	0.0150	0.0192
wolf \rightarrow lion	0.2990	0.0726	0.8856	0.2704	0.0291	0.2622	0.3014	0.0269	0.1827	0.2999	0.0253	0.0778
zebra \rightarrow horse	0.3006	0.0933	0.8659	0.2790	0.0379	0.6584	0.2944	0.0212	0.1372	0.2918	0.0189	0.1176
dog \rightarrow dog w/ glasses	0.3139	0.0689	0.3541	0.2960	0.0197	0.2342	0.3247	0.0104	0.0921	0.3240	0.0097	0.0139

4.1 Implementation Details

Our method is implemented using the publicly available official code of Pix2Pix-Zero [35] based on PyTorch [43] with a single NVIDIA A100 GPU. For faster inference of Stable Diffusion [26] using DDIM [4], we employ 50 steps for latent extraction in Eq. (1), and target image generation. We obtain a source prompt to employ the vision-language model BLIP [44] while a target prompt is made by replacing words in the source sentence according to a given task. For example, in case of the “dog-to-cat” task, if the source prompt is “a cute little white dog with blue eyes”, the target prompt is represented as “a cute little white cat with blue eyes”. When we generate target images, all comparison methods including the proposed method apply classifier-free guidance [45]. For fair comparisons, we run the official codes of Prompt-to-Prompt [33] and Pix2Pix-Zero [35] starting from the same final latent \mathbf{x}_T and the same target prompt when synthesizing target images.

4.2 Evaluation Metrics

To compare the proposed method with previous state-of-the-art techniques, we employ two widely used metrics from existing studies: CLIP-similarity (CS) [46] and structure distance (SD) [47]. CS assesses the alignment between the target image and the target prompt while SD estimates the overall structural disparity between the source and target images.

Furthermore, we introduce a novel metric referred to as relational distance (RD), which quantifies how faithfully the relational information between source images is preserved between translated target images. With an ideal image-to-image translation algorithm, the distance between two source images should closely match the distance between their corresponding target images. Note that this metric has proven successful in the context of knowledge distillation [48]. For the computation of distance between two images, we adopt Perceptual Loss [49]. For quantitative evaluation, we sample 250 images on the LAION 5B dataset [20] using CLIP retrieval [50].

4.3 Quantitative Results

Table 3 presents the results to compare with the state-of-the-art methods [33, 35] and the naive DDIM [4] inference using Eq. (3). As presented in the table, the proposed method outperforms the existing methods in terms of the CLIP-Sim and Structure Dist in most cases while the proposed method always achieves the lowest value of Relational Dist. Although Pix2Pix-Zero has higher values of CLIP-Sim, the proposed method preserves the structure more and our method is much more efficient in terms of memory and speed since we do not need to perform the backpropagation through the text-to-image diffusion model.

4.4 Qualitative Results

Figure 4 visualizes generated images given by reconstruction, the naive DDIM method using Eq. (3), Prompt-to-Prompt [33], Pix2Pix-Zero [35], and the proposed method. As illustrated in the figure, the proposed method can preserve the background while editing the content effectively. Note that Pix2Pix-Zero sometimes fail to maintain the structure as presented in the “cat-to-dog” task. On the other hand, the comparison methods often fail to maintain the structure. Also, we present additional qualitative results using synthesized images given by Stable Diffusion in Figure 5.

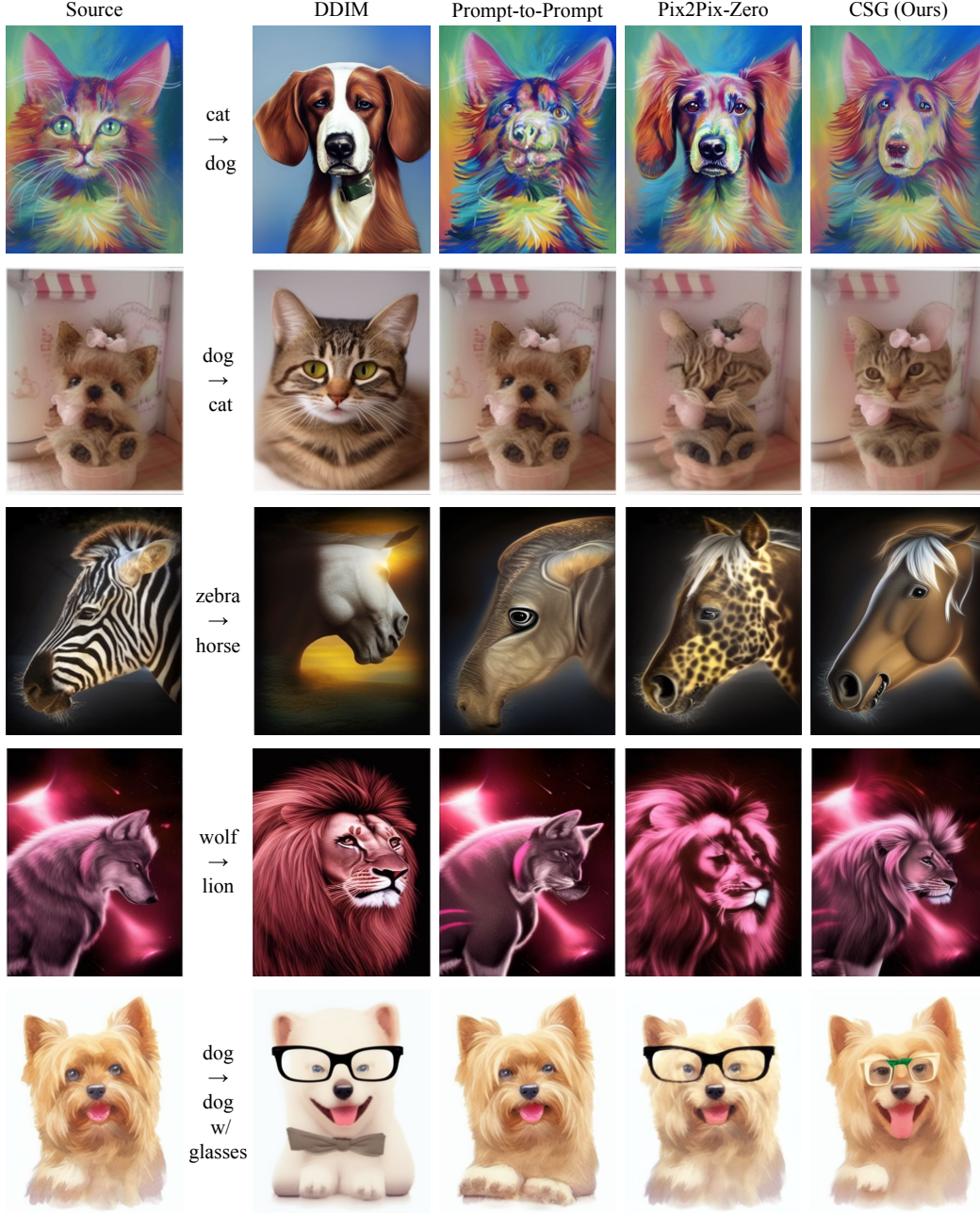


Figure 4: Qualitative results of the pretrained Stable Diffusion [26] using real images sampled from LAION 5B dataset [20] on various tasks. The proposed algorithm (CSG) illustrates high-fidelity translated images compared to other methods.

4.5 Ablation Study

Table 2 presents ablation study results from analyzing the effect of the proposed components on various tasks when implemented on top of the Stable Diffusion model. The table implies that using the conditional score guidance without using the cross-attention mixup in Eq. (6), ‘CSG w/o Mixup’ is helpful to preserve structures of source images compared with the naive DDIM. Furthermore, the cross-attention mixup enhances text-driven image manipulation performance when combined with the conditional score guidance.



Figure 5: Qualitative results of the proposed method using the pretrained Stable Diffusion [26] and its synthesized images for various tasks.

Table 2: Ablation study results from the LAION 5B dataset [20] for various tasks using the pretrained Stable Diffusion model [26]. ‘CSG w/o Mixup’ synthesizes target images without using the cross-attention mixup discussed in Eq. (6).

Task	DDIM [4]			CSG w/o Mixup			CSG		
	CS (\uparrow)	SD (\downarrow)	RD (\downarrow)	CS (\uparrow)	SD (\downarrow)	RD (\downarrow)	CS (\uparrow)	SD (\downarrow)	RD (\downarrow)
cat \rightarrow dog	0.2921	0.0725	0.4325	0.3008	0.0199	0.0229	0.3014	0.0192	0.0217
dog \rightarrow cat	0.2903	0.0748	0.4608	0.2959	0.0161	0.0226	0.2958	0.0150	0.0192
wolf \rightarrow lion	0.2990	0.0726	0.8856	0.3000	0.0273	0.0829	0.2999	0.0253	0.0778
zebra \rightarrow horse	0.3006	0.0933	0.8659	0.2916	0.0195	0.1231	0.2918	0.0189	0.1176
dog \rightarrow dog w/ glasses	0.3139	0.0689	0.3541	0.3238	0.0103	0.0654	0.3240	0.0097	0.0139

5 Conclusion

We proposed a training-free method using a pre-trained text-to-image diffusion model for text-driven image manipulation tasks. Different from existing methods relying on a simple score conditioned only on a target textual input, we formulated a conditional score conditioned on both a source image and a source text in addition to the target prompt. Our conditional score can be decomposed into the standard score easily calculated using the generative model and the gradient of the posterior of the source latent conditioned on the target latent and target prompt with respect to the target latent for manipulation. For the computation of the guiding term, we used a Gaussian distribution to model the posterior distribution, where its mean is simply set to the target latent while the precision matrix is estimated based on the background mask. To further boost the editing performance, a new cross-attention mixup method was incorporated into the conditional score guidance framework. Experimental results verify that the proposed method achieves outstanding performance in various text-driven image-to-image translation scenarios.

Acknowledgments This work was partly supported by LG AI Research.

References

- [1] Sohl-Dickstein, J., Weiss, E., Maheswaranathan, N., Ganguli, S.: Deep Unsupervised Learning using Nonequilibrium Thermodynamics. In ICML. (2015)
- [2] Ho, J., Jain, A., Abbeel, P.: Denoising Diffusion Probabilistic Models. In NeurIPS. (2020)
- [3] Song, Y., Sohl-Dickstein, J., Kingma, D.P., Kumar, A., Ermon, S., Poole, B.: Score-Based Generative Modeling through Stochastic Differential Equations. In ICLR. (2021)
- [4] Song, J., Meng, C., Ermon, S.: Denoising Diffusion Implicit Models. In ICLR. (2021)
- [5] Li, X., Thickstun, J., Gulrajani, I., Liang, P.S., Hashimoto, T.B.: Diffusion-LM Improves Controllable Text Generation. In NeurIPS. (2022)
- [6] Gong, S., Li, M., Feng, J., Wu, Z., Kong, L.: DiffuSeq: Sequence to Sequence Text Generation with Diffusion Models. In ICLR. (2023)
- [7] Gao, S., Zhou, P., Cheng, M.M., Yan, S.: Masked Diffusion Transformer is a Strong Image Synthesizer. arXiv preprint arXiv:2303.14389 (2023)
- [8] Dhariwal, P., Nichol, A.: Diffusion Models Beat GANs on Image Synthesis. In NeurIPS. (2021)
- [9] Choi, J., Kim, S., Jeong, Y., Gwon, Y., Yoon, S.: ILVR: Conditioning Method for Denoising Diffusion Probabilistic Models. In ICCV. (2021)
- [10] Saharia, C., Chan, W., Chang, H., Lee, C., Ho, J., Salimans, T., Fleet, D., Norouzi, M.: Palette: Image-to-Image Diffusion Models. In SIGGRAPH. (2022)
- [11] Tumanyan, N., Geyer, M., Bagon, S., Dekel, T.: Plug-and-Play Diffusion Features for Text-Driven Image-to-Image Translation. In CVPR. (2023)
- [12] Lin, C.H., Gao, J., Tang, L., Takikawa, T., Zeng, X., Huang, X., Kreis, K., Fidler, S., Liu, M.Y., Lin, T.Y.: Magic3D: High-Resolution Text-to-3D Content Creation. In CVPR. (2023)
- [13] Poole, B., Jain, A., Barron, J.T., Mildenhall, B.: DreamFusion: Text-to-3D using 2D Diffusion. In ICLR. (2023)
- [14] Tevet, G., Raab, S., Gordon, B., Shafir, Y., Cohen-or, D., Bermano, A.H.: Human Motion Diffusion Model. In ICLR. (2023)
- [15] Kim, J., Kim, J., Choi, S.: Flame: Free-form Language-based Motion Synthesis & Editing. In AAAI. (2023)
- [16] Ho, J., Chan, W., Saharia, C., Whang, J., Gao, R., Gritsenko, A., Kingma, D.P., Poole, B., Norouzi, M., Fleet, D.J., et al.: Imagen Video: High Definition Video Generation with Diffusion Models. arXiv preprint arXiv:2210.02303 (2022)
- [17] Qi, C., Cun, X., Zhang, Y., Lei, C., Wang, X., Shan, Y., Chen, Q.: Fatezero: Fusing attentions for zero-shot text-based video editing. arXiv preprint arXiv:2303.09535 (2023)
- [18] Yang, D., Yu, J., Wang, H., Wang, W., Weng, C., Zou, Y., Yu, D.: Diffsound: Discrete Diffusion Model for Text-to-Sound Generation. TASLP (2023)
- [19] Huang, R., Zhao, Z., Liu, H., Liu, J., Cui, C., Ren, Y.: ProDiff: Progressive Fast Diffusion Model for High-Quality Text-to-Speech. In ACMM. (2022)
- [20] Schuhmann, C., Beaumont, R., Vencu, R., Gordon, C.W., Wightman, R., Cherti, M., Coombes, T., Katta, A., Mullis, C., Wortsman, M., et al.: LAION-5B: An open large-scale dataset for training next generation image-text models. In NeurIPS Datasets and Benchmarks Track. (2022)
- [21] Sharma, P., Ding, N., Goodman, S., Soricut, R.: Conceptual Captions: A Cleaned, Hypernymed, Image Alt-text Dataset For Automatic Image Captioning. In ACL. (2018)

- [22] Changpinyo, S., Sharma, P., Ding, N., Soricut, R.: Conceptual 12m: Pushing Web-Scale Image-Text Pre-training To Recognize Long-Tail Visual Concepts. In CVPR. (2021)
- [23] Thomee, B., Shamma, D.A., Friedland, G., Elizalde, B., Ni, K., Poland, D., Borth, D., Li, L.J.: YFCC100M: The New Data in Multimedia Research. Communications of the ACM (2016)
- [24] Byeon, M., Park, B., Kim, H., Lee, S., Baek, W., Kim, S.: Coyo-700m: Image-text pair dataset. <https://github.com/kakaobrain/coyo-dataset> (2022)
- [25] Saharia, C., Chan, W., Saxena, S., Li, L., Whang, J., Denton, E.L., Ghasemipour, K., Gontijo Lopes, R., Karagol Ayan, B., Salimans, T., et al.: Photorealistic Text-to-Image Diffusion Models with Deep Language Understanding. In NeurIPS. (2022)
- [26] Rombach, R., Blattmann, A., Lorenz, D., Esser, P., Ommer, B.: High-Resolution Image Synthesis with Latent Diffusion Models. In CVPR. (2022)
- [27] Nichol, A., Dhariwal, P., Ramesh, A., Shyam, P., Mishkin, P., McGrew, B., Sutskever, I., Chen, M.: Glide: Towards Photorealistic Image Generation and Editing with Text-Guided Diffusion Models. In ICML. (2022)
- [28] Ramesh, A., Dhariwal, P., Nichol, A., Chu, C., Chen, M.: Hierarchical Text-Conditional Image Generation with CLIP Latents. arXiv preprint arXiv:2204.06125 (2022)
- [29] Gu, S., Chen, D., Bao, J., Wen, F., Zhang, B., Chen, D., Yuan, L., Guo, B.: Vector Quantized Diffusion Model for Text-to-Image Synthesis. In CVPR. (2022)
- [30] Meng, C., He, Y., Song, Y., Song, J., Wu, J., Zhu, J.Y., Ermon, S.: SDEdit: Guided Image Synthesis and Editing with Stochastic Differential Equations. In ICLR. (2021)
- [31] Kim, G., Kwon, T., Ye, J.C.: DiffusionCLIP: Text-Guided Diffusion Models for Robust Image Manipulation. In CVPR. (2022)
- [32] Avrahami, O., Lischinski, D., Fried, O.: Blended Diffusion for Text-Driven Editing of Natural Images. In CVPR. (2022)
- [33] Hertz, A., Mokady, R., Tenenbaum, J., Aberman, K., Pritch, Y., Cohen-or, D.: Prompt-to-Prompt Image Editing with Cross-Attention Control. In ICLR. (2023)
- [34] Kawar, B., Zada, S., Lang, O., Tov, O., Chang, H., Dekel, T., Mosseri, I., Irani, M.: Imagic: Text-Based Real Image Editing with Diffusion Models. In CVPR. (2023)
- [35] Parmar, G., Singh, K.K., Zhang, R., Li, Y., Lu, J., Zhu, J.Y.: Zero-Shot Image-to-Image Translation. arXiv preprint arXiv:2302.03027 (2023)
- [36] Van Den Oord, A., Vinyals, O., et al.: Neural Discrete Representation Learning. In NIPS. (2017)
- [37] Esser, P., Rombach, R., Ommer, B.: Taming Transformers for High-Resolution Image Synthesis. In CVPR. (2021)
- [38] Radford, A., Kim, J.W., Hallacy, C., Ramesh, A., Goh, G., Agarwal, S., Sastry, G., Askell, A., Mishkin, P., Clark, J., et al.: Learning Transferable Visual Models from Natural Language Supervision. In ICML. (2021)
- [39] Raffel, C., Shazeer, N., Roberts, A., Lee, K., Narang, S., Matena, M., Zhou, Y., Li, W., Liu, P.J.: Exploring the Limits of Transfer Learning with a Unified Text-to-Text Transformer. JMLR (2020)
- [40] Gal, R., Patashnik, O., Maron, H., Bermano, A.H., Chechik, G., Cohen-Or, D.: StyleGAN-NADA: CLIP-Guided Domain Adaptation of Image Generators. TOG (2022)
- [41] Deng, J., Guo, J., Xue, N., Zafeiriou, S.: Arcface: Additive Angular Margin Loss for Deep Face Recognition. In CVPR. (2019)

- [42] Ronneberger, O., Fischer, P., Brox, T.: U-Net: Convolutional Networks for Biomedical Image Segmentation. In MICCAI. (2015)
- [43] Paszke, A., Gross, S., Massa, F., Lerer, A., Bradbury, J., Chanan, G., Killeen, T., Lin, Z., Gimelshein, N., Antiga, L., et al.: PyTorch: An Imperative Style, High-Performance Deep Learning Library. In NeurIPS. (2019)
- [44] Li, J., Li, D., Xiong, C., Hoi, S.: BLIP: Bootstrapping Language-Image Pre-training for Unified Vision-Language Understanding and Generation. In ICML. (2022)
- [45] Ho, J., Salimans, T.: Classifier-Free Diffusion Guidance. In NeurIPS Workshop on Deep Generative Models and Downstream Applications. (2021)
- [46] Hessel, J., Holtzman, A., Forbes, M., Bras, R.L., Choi, Y.: CLIPScore: a reference-free evaluation metric for image captioning. In EMNLP. (2021)
- [47] Tumanyan, N., Bar-Tal, O., Bagon, S., Dekel, T.: Splicing ViT Features for Semantic Appearance Transfer. In CVPR. (2022)
- [48] Park, W., Kim, D., Lu, Y., Cho, M.: Relational Knowledge Distillation. In CVPR. (2019)
- [49] Johnson, J., Alahi, A., Fei-Fei, L.: Perceptual Losses for Real-Time Style Transfer and Super-Resolution. In ECCV. (2016)
- [50] Beaumont, R.: Clip Retrieval: Easily compute clip embeddings and build a clip retrieval system with them. <https://github.com/rom1504/clip-retrieval> (2022)
- [51] Zhang, R., Isola, P., Efros, A.A., Shechtman, E., Wang, O.: The Unreasonable Effectiveness of Deep Features as a Perceptual Metric. In CVPR. (2018)

Table 3: Additional quantitative results to compare with text-driven image-to-image translation methods [4, 33, 35] using the pre-trained Stable Diffusion [26] and real images sampled from LAION 5B dataset [20] for various tasks. ‘DDIM’ denotes the simple inference using Eq. (16). Black and red bold-faced numbers represent the best and second-best performance in each row.

Task	DDIM [4]	Prompt-to-Prompt [33]	Pix2Pix-Zero [35]	CSG (Ours)
	BG-LPIPS (\downarrow)	BG-LPIPS (\downarrow)	BG-LPIPS (\downarrow)	BG-LPIPS (\downarrow)
cat \rightarrow dog	0.3834	0.2343	0.2111	0.1867
dog \rightarrow cat	0.3602	0.2954	0.1983	0.1645
wolf \rightarrow lion	0.4042	0.3153	0.2402	0.2384
zebra \rightarrow horse	0.4127	0.2932	0.2312	0.2303
dog \rightarrow dog w/ glasses	0.3247	0.1616	0.1037	0.1121

A Appendix

This document first presents additional quantitative results to show the effectiveness of the proposed method by measuring the background difference between source and target images using Learned Perceptual Image Patch Similarity metric [51] referred to as BG-LPIPS. Then, we demonstrate additional qualitative results of CSG compared with the state-of-the-art methods [4, 33, 35]. Finally, we formulate our introduced metric about relational distance (RD).

A.1 Additional Quantitative Results

In addition to Table 1 of the main paper using CLIP-similarity [46], structure distance [47], and relational distance, we report BG-LPIPS of the proposed method and existing frameworks [4, 33, 35] for evaluation. As presented in Table 3, CSG achieves the lowest BG-LPIPS in most tasks, which implies that the proposed method preserves the background region better.

A.2 Additional Qualitative Results

We provide additional qualitative results using real images sampled from the LAION 5B dataset [20] in Figure 6, 7, 8, 9, and 10, which implies the superiority of CSG compared with the state-of-the-art methods [4, 33, 35]. Figure 11 and 12 also demonstrate that the proposed method achieves outstanding performance on synthesized images given by the pre-trained Stable Diffusion [26].

A.3 Relational Distance

RD is introduced to measure how faithfully the relational information between source images is preserved between synthesized target images, which is given by

$$RD = \min_{\gamma} \frac{1}{n} \|G^{\text{tgt}} - \gamma G^{\text{src}}\|_F^2, \quad (17)$$

where $\|\cdot\|_F$ denotes the Frobenius norm. In the above equation, G^{tgt} and G^{src} are $n \times n$ matrices, where the entry $G^{\text{tgt}}[i, j]$ in the i^{th} row and j^{th} column of a matrix G^{tgt} is the perceptual distance [49] between i^{th} and j^{th} target images while $G^{\text{src}}[i, j]$ is the perceptual distance between i^{th} and j^{th} source images.



Figure 6: Additional qualitative results of the Stable Diffusion [26] using real images sampled from LAION 5B dataset [20] on the cat-to-dog task.



Figure 7: Additional qualitative results of the Stable Diffusion [26] using real images sampled from LAION 5B dataset [20] on the dog-to-cat task.

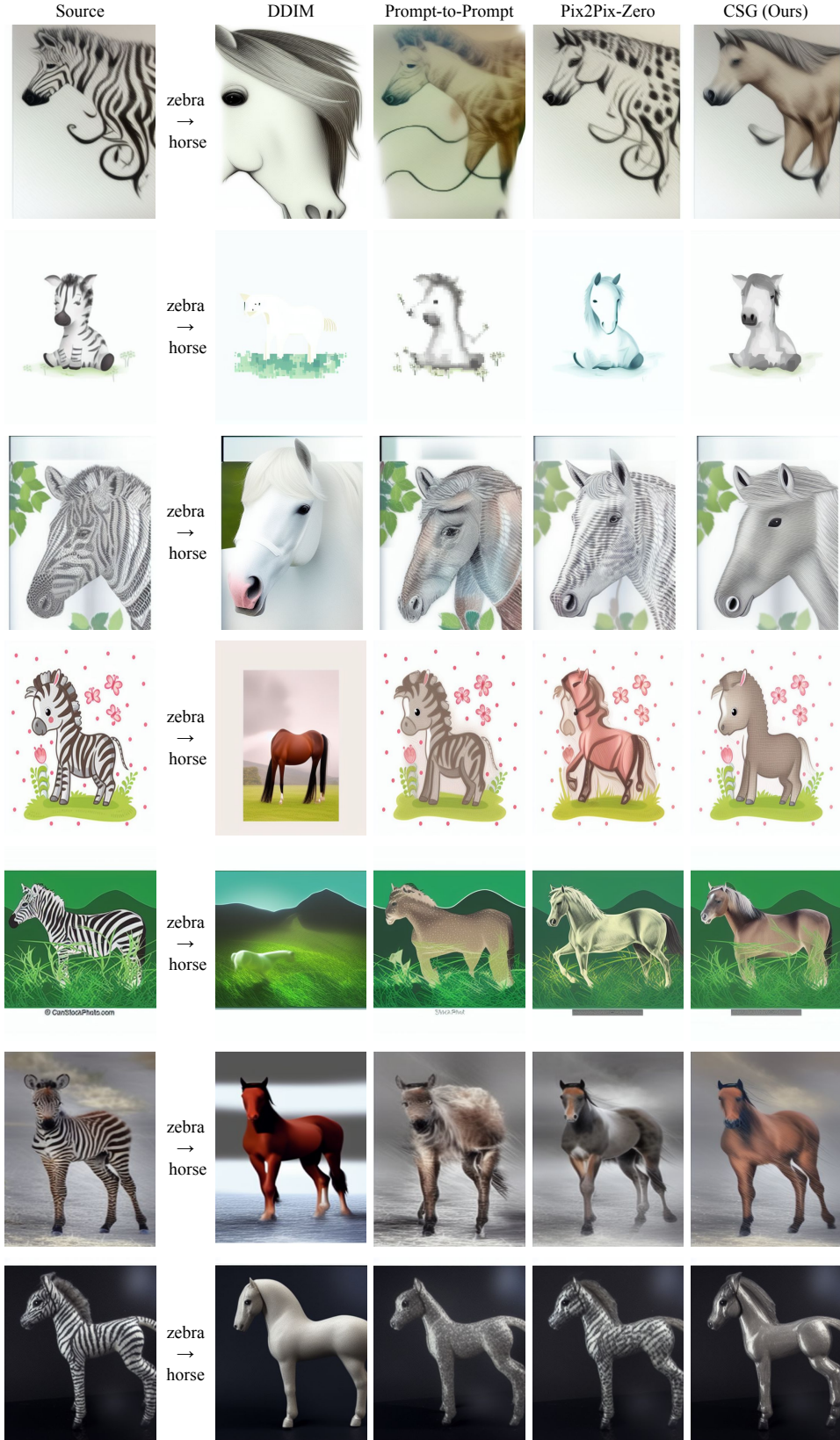


Figure 8: Additional qualitative results of the Stable Diffusion [26] using real images sampled from LAION 5B dataset [20] on the zebra-to-horse task.

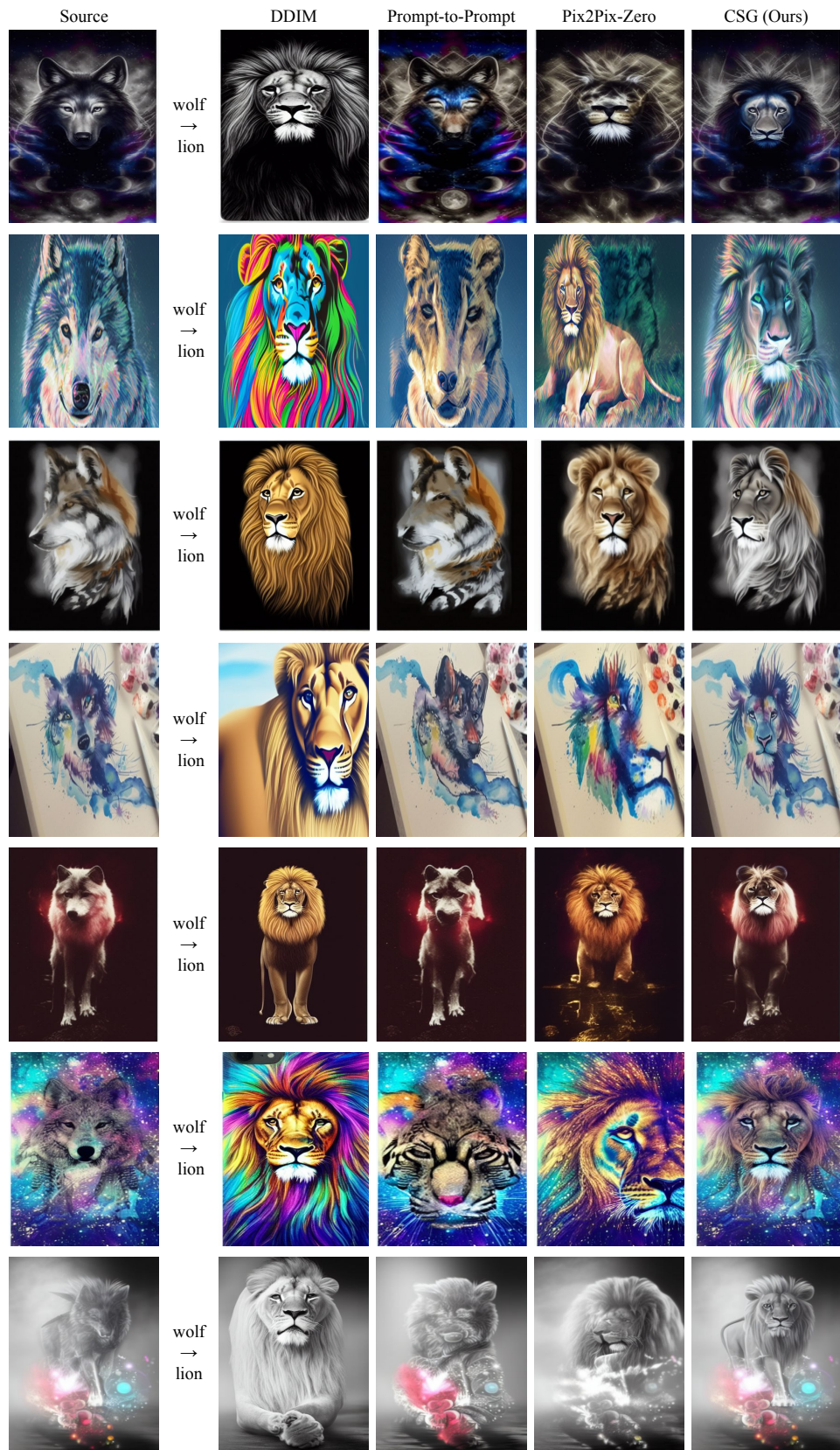


Figure 9: Additional qualitative results of the Stable Diffusion [26] using real images sampled from LAION 5B dataset [20] on the wolf-to-lion task.



Figure 10: Additional qualitative results of the Stable Diffusion [26] using real images sampled from LAION 5B dataset [20] on the dog-to-dog w/ glasses task.

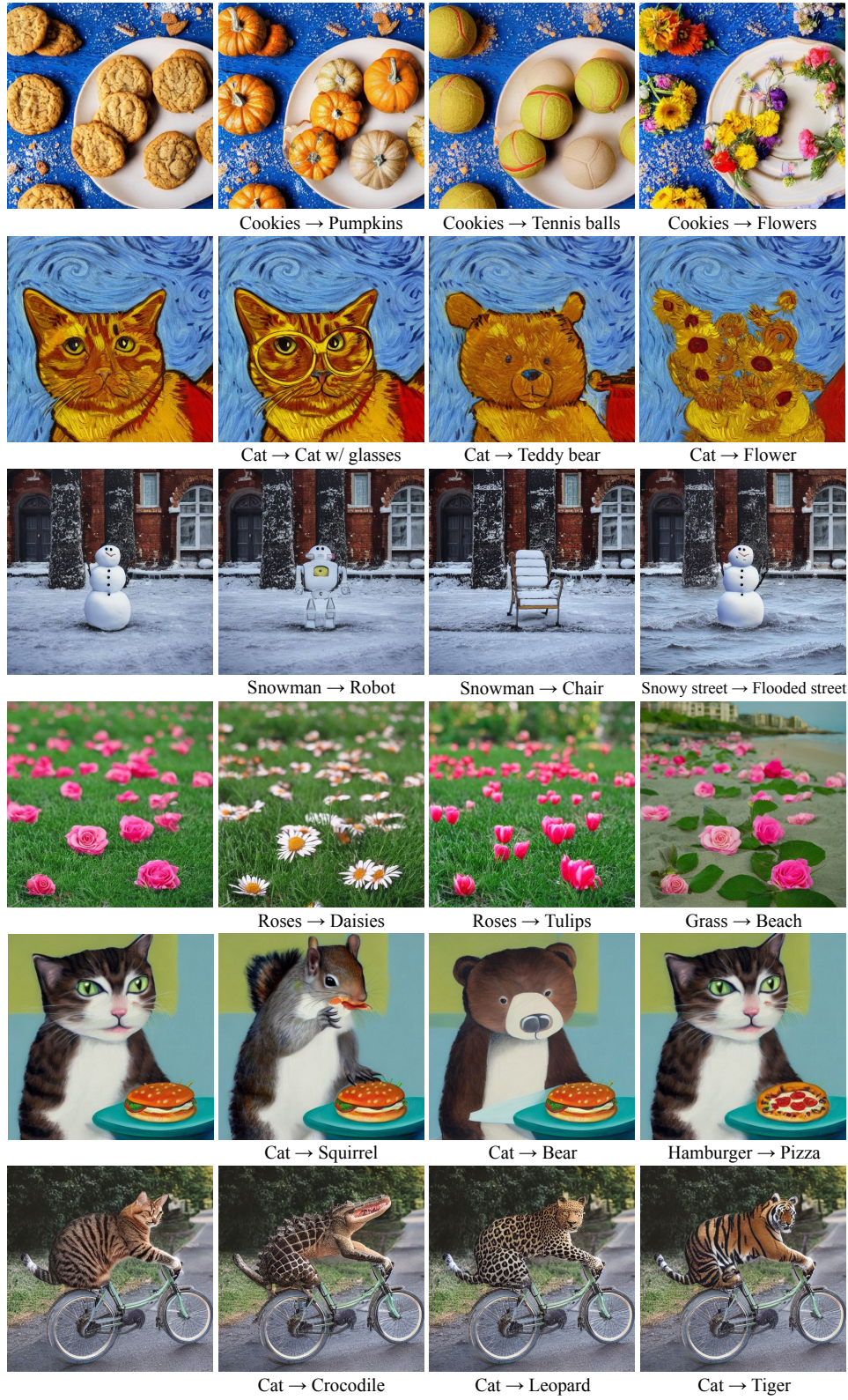


Figure 11: Additional qualitative results of the proposed method using the pre-trained Stable Diffusion [26] and its synthesized images for various tasks.

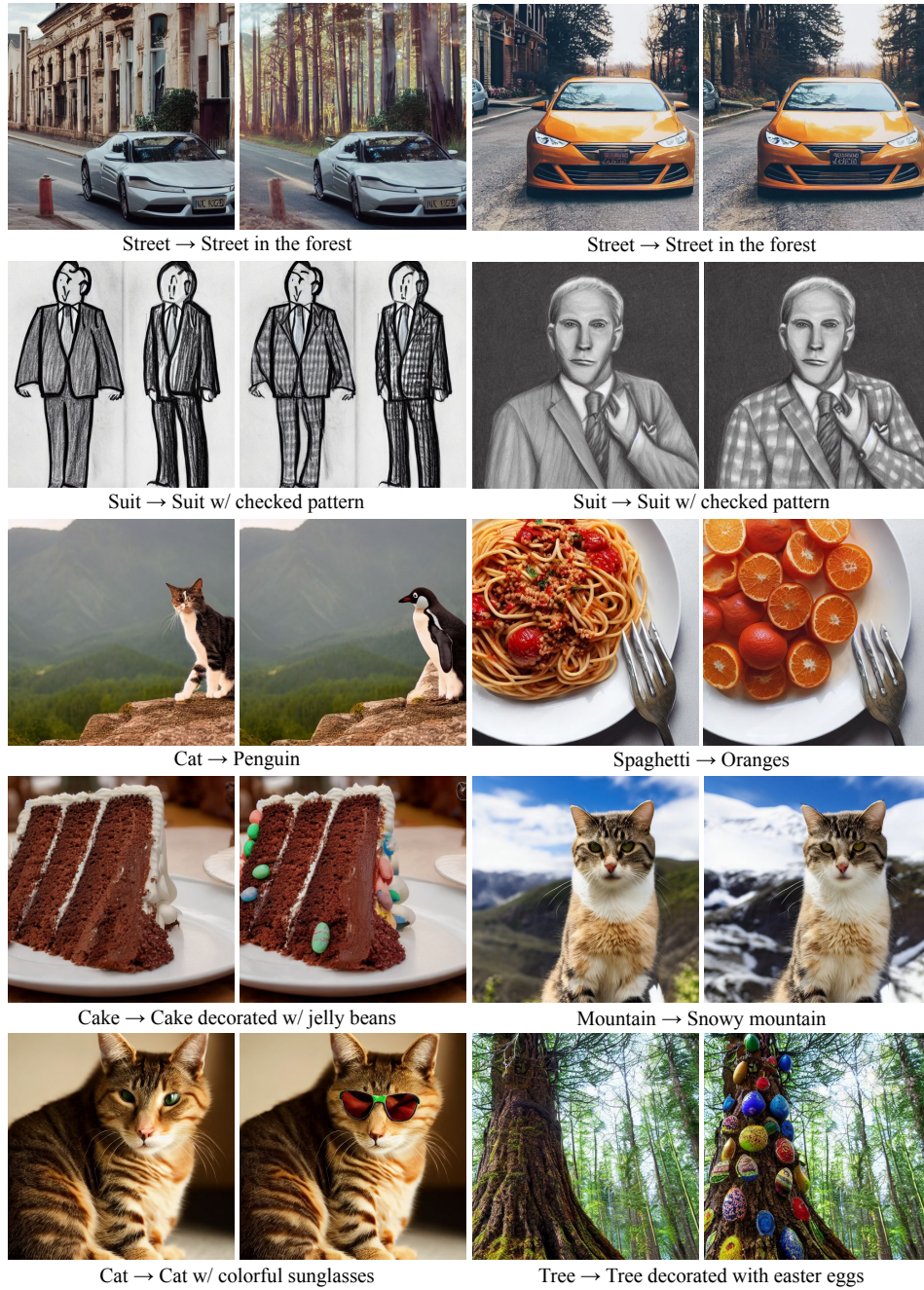


Figure 12: Additional qualitative results of the proposed method using the pre-trained Stable Diffusion [26] and its synthesized images for various tasks.